ISSN:0971-3093



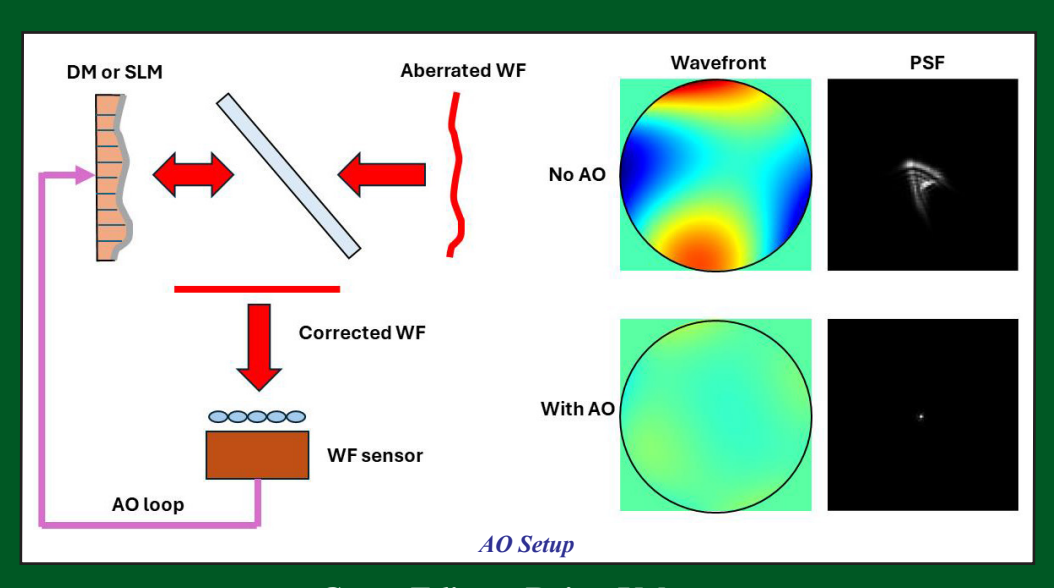
Vol 33, Nos 5-6, May-June, 2024

# ASIAN JOURNAL OF PHYSICS

# An International Peer Reviewed Research Journal

Advisory Editors: W Kiefer, FTS Yu, Maria J Yzuel

Special issue on "Adaptive Optics and Wavefront Sensing"



Guest Editor: Brian Vohnsen



# **ANITA PUBLICATIONS**

FF-43, 1st Floor, Mangal Bazar, Laxmi Nagar, Delhi-110 092, India B O: 2, Pasha Court, Williamsville, New York-14221-1776, USA



# **Asian Journal of Physics**

Vol. 33, Nos 5 & 6 (2024) 411-418





# Sensing wavefront aberrations using intensity gradients

Brian Vohnsen<sup>1</sup>, Denise Valente dos Santos<sup>2</sup>, and Diego Rativa<sup>3</sup>

<sup>1</sup>Optics Group, School of Physics, University College Dublin, Dublin 4, Ireland

<sup>2</sup>Fisica de Materiais, University of Pernambuco, Recife, PE, Brazil

<sup>3</sup>Institute of Technological Innovation, University of Pernambuco, Recife, PE, Brazil

Light propagation is governed by the optical wavefront and is vital to describe the performance and quality of any optical system. The wavefront represents a 2-D surface of in-phase points. It is commonly described by a function that depends on the cartesian (x, y) or radial  $(r, \theta)$  pupil coordinates. For convenience this can be projected onto orthogonal functions such as the Zernike polynomials which is the approach we will take.

There are different methods available to characterize wavefronts each with their pros and cons. Interferometric methods are useful for high precision tasks but are complicated by the fact that phase unwrapping is usually needed to reconstruct the measured wavefront. The wavefront may also be probed at multiple planes where comparative analysis can then reveal its shape. Alternatively, local wavefront sampling is often used for fast sensing tasks. The sampling can be accomplished by apertures, lenslets, fibre arrays, sectored pupils, refractive pyramids, etc. These may be physical objects but can also be realized by means of programmable spatial light modulators offering greater flexibility.

Ultimately, the wavefront phase impacts on intensity distributions and, therefore, several techniques have been developed that rely entirely or predominantly on intensity variations to determine the wavefront. In this contribution, we review intensity-based wavefront sensors developed in our laboratory from fibre-guided arrays, sequential wavefront sensing, to quasi-resonant sensors that all allow reconstruction of the probed wavefront. We also discuss some of the applications where the developed sensors may prove beneficial. © Anita Publications. All rights reserved.

doi: 10.54955.AJP.33.5-6.2024.411-418

**Keywords**: Wavefront sensors, Intensity gradients, Aberrations, Adaptive optics, Dynamic range, Sensitivity.

### 1 Introduction

Precise knowledge of the wavefront is essential for the understanding of light propagation, enhancing focusing capabilities, and optimizing imaging properties in the design of optical systems". Typically, it is most desirable to have either planar or spherical wavefronts as these can be easily controlled and manipulated to provide high optical quality [1]. The sensing of optical wavefronts is critical in applications that range from astronomy and microscopy to quality control and ophthalmology. Uncontrolled wavefront variations can significantly degrade optical performance and thereby lower quality metrics. This can blur images and ultimately reduce optical performance to an unacceptable level. In vision, the same holds true and vision corrections with eyeglasses or contact lenses may sometimes be compromised. More challenging wavefronts with higher-order aberrations, that cannot be corrected with lenses, can be corrected with phase plates when they are static in time or with adaptive optics when aberrations are changing in real time. This happens in astronomy with atmospheric fluctuations altering the refractive index of the air [2], and it happens in biosamples when performing microscopy of living organisms or cells [3]. In ophthalmology, it happens when the tear film breaks down [4] and when the direction of gaze is continuously changed [5].

Corresponding author

e mail: brian.vohnsen@ucd.ie (Brian Vohnsen)

When sensing aberrations, interferometric techniques offer high sensitivity but are complicated by the need of phase unwrapping methods. Alternative options include imaging of multiple planes to determine propagation directions as used in wavefront phase imaging [6]. Relatedly, a technique known as curvature sensing [7], uses brightness differences across different planes and computational techniques to determine the wavefront. Another option is the use of a refractive pyramid [8,9] to create multiple pupil images where local brightness differences can be used to determine the wavefront tilt. A pointed axicon [10] has been used with resemblance to a point-diffraction interferometer [11,12]. In this contribution, we will discuss techniques we have developed in our laboratories that use intensity gradients to determine wavefront aberrations, namely, waveguided wavefront sensors [13], sequential wavefront sensors [14,15], and quasi-resonant wavefront sensors [16,17].

### 2 Sensing of aberrations using optical waveguides

The work on using the angular selectivity of coupling of light to waveguides was inspired by our work on photoreceptor directionality. The cone photoreceptors of the human eye exhibit sensitivity to the angle at which light intersects the retina, a phenomenon referred to as the Stiles-Crawford effect [18,19]. This sensitivity drops of as a Gaussian function for single mode cylindrical waveguides (V number less than 2.405) but becomes more uniform for multimodal waveguides. The angular selectivity for a single waveguide is shown schematically in Fig 1. The power coupling of the transmission to guided light can be written an overlap integral between the field of the mode  $\psi_m$  and the incident wavefront  $\psi_i$  as expressed by Eq (1).



Fig 1. Coupling of a beam of light is dependent on the wavefront match between the incident light and that of the guided mode(s).

For the single-mode step-index cylindrical waveguide illuminated by an oblique plane wave, this can largely be written as a Gaussian function given by Eq (2) as a function of the angle of incidence  $\theta$  (in radians)

$$T(\theta) \sim \exp\left(\frac{-2\pi w_m^2}{\lambda^2}\theta^2\right)$$
 (2)

where  $w_m$  is the mode radius. If the incident wavefront is a beam, the exponent is modified but the angular dependence remains Gaussian [19]. Thus, for oblique light the transmitted intensity drops off and this can be used for sensing of the incident wavefront slope locally. In that case, a bias angle  $\theta_0$  should be chosen so that wavefront slopes can be larger or smaller than the initial angle. In the below configuration, we operated it with a bias angle of 4°. This was first done in the x-direction only, and subsequently in the y-direction to obtain wavefront slopes in both the x- and y-directions.

While it is possible to move the fibre across the wavefront to sequentially capture it, we opted to use an array of waveguides, employing an LMA-20 photonic crystal fibre (PCF) featuring a dense

arrangement of 126 cylindrical waveguides. The holes were filled with castor oil, which could be adjusted through temperature to ensure that each column of oil functioned as a single-mode or low-mode-number fibre Here, we chose to operate with a V number of 2.89 allowing two modes to be coupled to flatten slightly the angular response and decrease its sensitivity to misalignments and diameter fluctuations. The waveguides were sufficiently separated in the crystal to have negligible crosstalk between them. We used a deformable mirror (Boston MicromachinesTM) operated in closed adaptive optics loop with a Hartmann-Shack wavefront sensor (HS-WFS) to generate small and controllable amounts of monochromatic aberrations by sensing the transmitted light intensity across the PCF with a camera. Telescopic 4-f systems were used to image the deformable mirror onto the entrance facet of the PCF and onto the pupil of the HS-WFS [13]. Intensity images captured with the camera using controlled amounts of aberrations are shown in Fig 2 for different cases of induced monochromatic aberrations with the adaptive optics system.

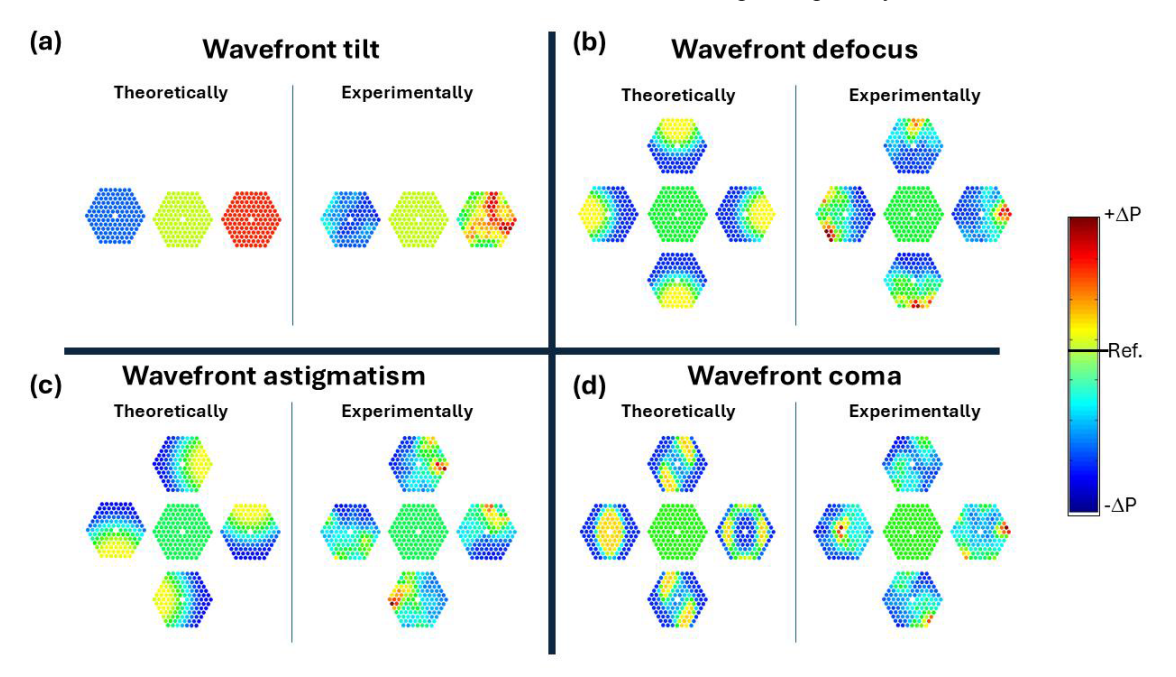


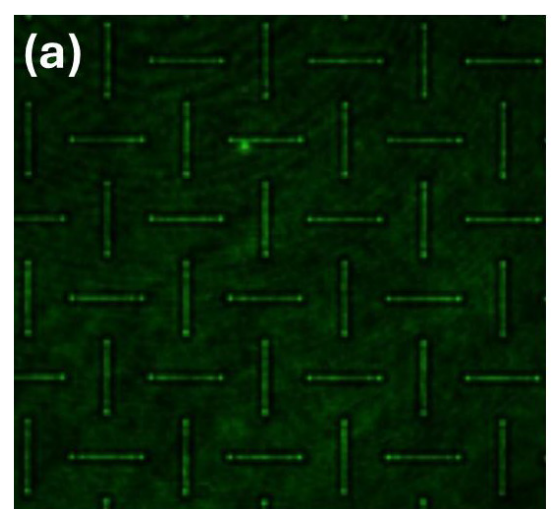
Fig 2. Examples of aberration sensing using the liquid-filled PCF to capture monochromatic aberrations. The cases present a comparison between the theoretical predictions for the waveguide array and the experimentally captured intensity images of transmitted waveguided light in cases of: (a) wavefront tilt, (b) wavefront defocus, (c) wavefront astigmatism, and (d) wavefront coma. The figure has been adapted with permission from [13] © Optical Society of America.

To eliminate the need for separately capturing the wavefront slopes in two dimensions, one could create arrays of adjacent waveguides with entrance facets clipped at the desired bias angle and oriented in the intended direction. With such an arrangement it would be possible to capture the wavefront without adjusting the bias angle.

As a follow-up project we looked at 3-D printed waveguides produced with NanoScribeTM and waveguides produced in AZ40XT photoresist. We aimed to create narrow slab waveguides that would only allow one of few modes in the narrow direction, but many modes in the wide direction. This would permit capturing of the intensity (using the large width) and the wavefront (using the narrow width). Examples of such structures are shown in Fig 3. Although the photoresist worked well, our focus moved onto retinal implants where they could serve to guide light for patients suffering from retinitis pigmentosa

and photoreceptor loss [20]. In turn, the large aspect ratio of the 3-D printed structures caused problems with stability, and they would often collapse or break when handled.

In summary, key advantages of a waveguide-based sensor resembling an endoscope is that it could potentially be operated in liquid environments and at angles to access places where it may otherwise be difficult to capture the wavefront. However, it would need further development and refinement beyond the proof-of-principle that we presented here.



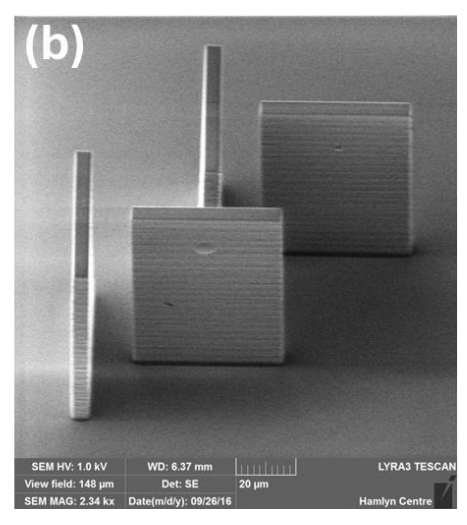


Fig 3. Examples of rectangular waveguides created in (a) photoresist film illuminated by laser light at 543 nm wavelength, and (b) with 3-D printing of waveguide structures herewith shown with electron microscopy.

### 3 Sensing of aberrations using sequential scanning

Another sensing technique that we explored was based on the HS-WFS wavefront sensor but with elimination of the problem of crosstalk. Crosstalk may occur when light from one lens in the lenslet array overlaps with light from an adjacent lens, thereby degrading the accuracy of wavefront reconstruction. To handle this, we developed a wavefront sensor using an aperture created by a Digital Micromirror Device (DMD) Vialux V-7001 that operated at a speed of 22.727 kHz and with  $1024 \times 768$  micromirrors each of size 13.7 µm. In this case, no lenslet array was needed since only one point-spread-function (PSF) would be captured at any time by the camera. The sensor would sequentially capture the entire wavefront  $\phi$  by raster scanning a square aperture of size (w×w) across the DMD. For each aperture the centroid coordinates of the PSF could be determined using the same approach as done with conventional HS-WFS. Equation (3) expresses the PSF determined by a square aperture centered at coordinates ( $x_0$ ,  $y_0$ ).

$$PSF \propto \left| FT \left\{ rect \left( \frac{x - x_0}{w} \right) \right\} rect \left( \frac{y - y_0}{w} \right) exp(i\phi) \right|^2$$
(3)

The system was tested and validated using the same adaptive optics loop as used with the waveguide-based wavefront sensor described in Section 2. An example of reconstructed Zernike wavefronts with the sensor is shown in Fig 4. The system was able to reconstruct the lower-order aberrations very well but showed more variability and less range for the higher-order aberrations. This is partly due to the limited stroke of the deformable mirror in the adaptive optics loop, as well as the restricted sampling when scanning the pupil with the DMD, with a sparse 5×5 aperture array. A slight asymmetry is seen, which relates to the DMD being placed at an angle to allow the reflected light of the 'on' micromirrors to enter the optical path of the system and the 'off' micromirrors reflecting light out of the system. When desiring higher accuracy,

more and smaller apertures with the DMD can easily be coded into the system, potentially even with some spatial overlap, but at the cost of a reduction in the speed of the sensor.

In a subsequent study, we used the same system to measure the ocular aberrations including cases of high myopia, and the system was capable of reconstructing defocus value in agreement with expectations [15].

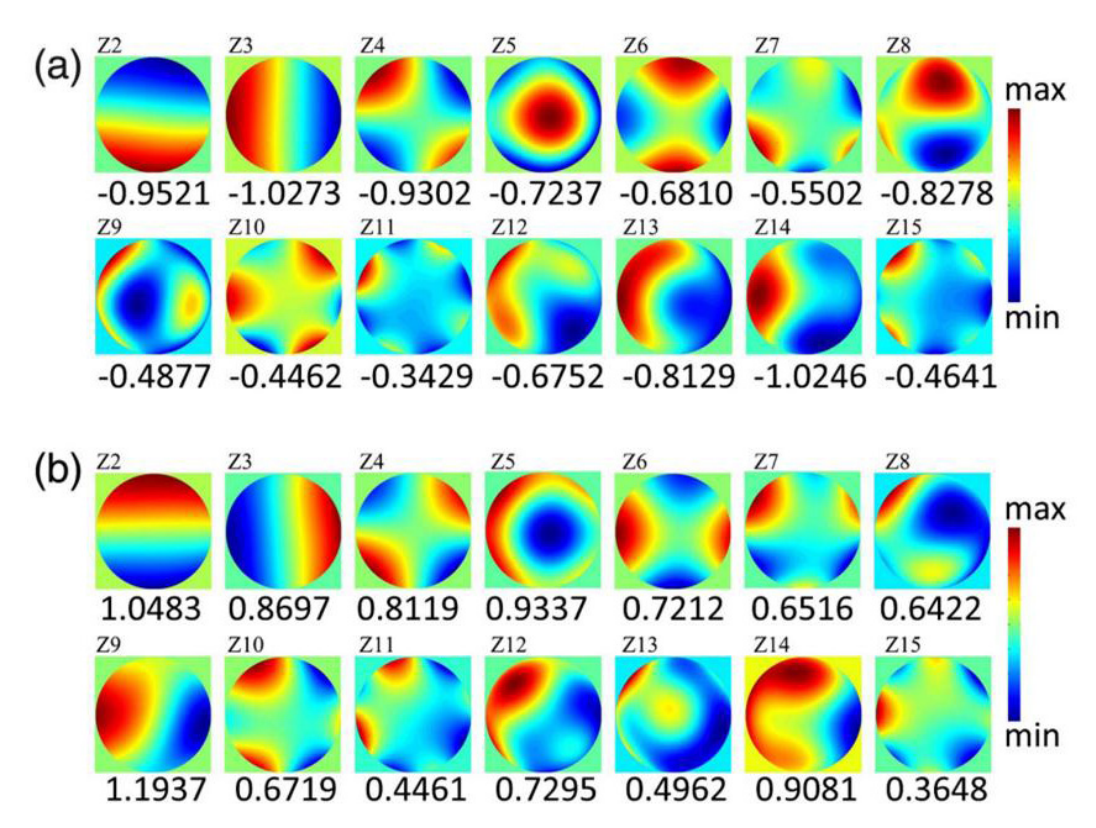


Fig 4. Example of wavefront reconstruction using a crosstalk-free HS-WFS with raster scanning of the wavefront. Individual Zernike coefficients of  $\pm 1~\mu m$  amplitude were generated and reconstructed with the sensor. In (a) negative Zernike coefficients were generated and in (b) positive Zernike coefficients were generated. The values below each figure show the magnitude of the reconstruction. The figure has been adapted with permission from [14] © Optical Society of America.

### 4 Sensing of aberrations using quasi-resonant interactions

The intensity-based sensors described above have been spatially limited by the sampling array of the HS-WFS, the sampling array of the DMD, and by the sampling array of the PCF. We developed a very different approach using quasi-resonant interactions between light and a structure [16]. The interaction could be a Bragg reflector or another highly angular sensitive interaction, but we chose to test the method using a slightly off-resonant reflection from 50 nm thin gold films by excitation of surface plasmon polaritons with p-polarized light. This was done in the Kretschmann configuration where light is incident via a prism by total internal reflection, and the surface plasmon polariton is noted by a reduction in the reflectivity of the gold film. The method is shown schematically in Fig 5. Like the situation with the bias angle for the waveguide-based sensor described in Section 2, it was necessary to operate the sensor slightly outside of

the optimal surface plasmon excitation angle on the negative (configuration I) or positive (configuration II) slope of the reflectance curve. The dynamic range and the sensitivity of the sensor could be altered using other film thicknesses or metals for the surface plasmon excitation.

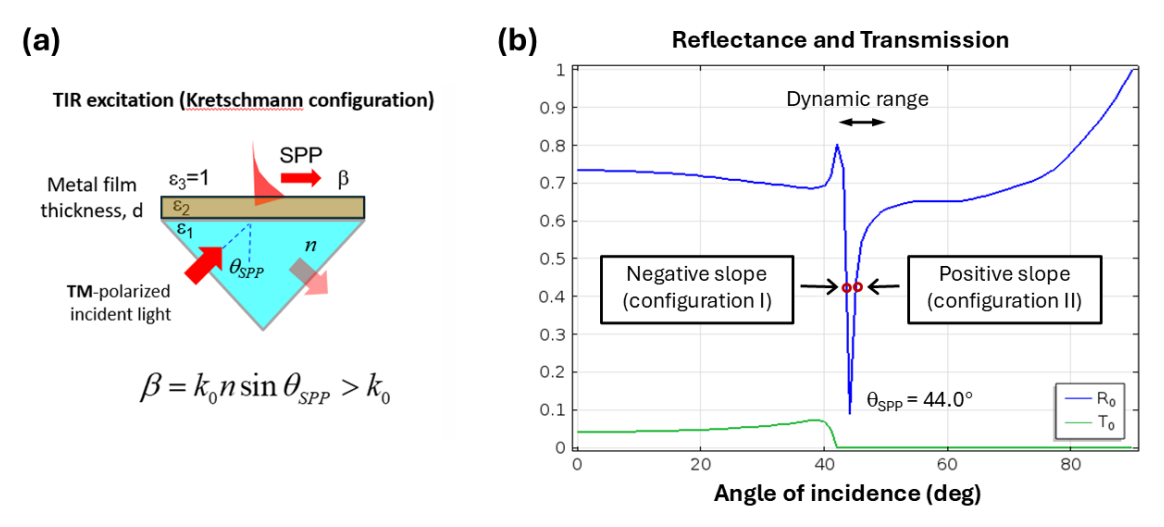


Fig 5. Excitation of a surface plasmon polariton (a) at the interface between a thin gold film and air using the Kretschmann configuration, and (b) the resulting transmission (green) and reflection (blue) curves. The figure has been adapted with permission from [16] © Optical Society of America.

To validate the sensor method, wavefronts were induced and controlled with the adaptive optics loop used also in Sections 2 and 3. A camera was located to capture the entire beam cross section across the reflected light whereby aberrations in the beam would translate into brightness differences across the image corresponding to slightly different angles of incidence as set determined by the aberrations. If no aberrations were present, the angle of incidence would be the same across the full width of the beam. Thus, this could be used as a reference image for the wavefront determination with aberrations.

Two sets of images had to be captured as the sensor would only see wavefront slopes in the plane of incidence. To capture the slope of wavefronts out of the plane the system could be rotated and images captured in a vertical direction out of the plane. Thus, the sensor captures essentially images of the cartesian derivates of the wavefront. This could potentially be avoided, by using embossing of microprisms at alternating orientations to capture simultaneously both the x and y-derivates of the wavefront in a single image in a similar manner to the rectangular waveguides in Section 2.

Figure 6 shows reconstructed Zernike wavefronts with the sensor operating in both configurations I and II, i.e., slightly below and above the resonance angle for the surface plasmon polariton excitation. The raw CCD images show the cartesian x and y-derivatives of the Zernike polynomials. The reconstructed wavefronts are not perfect but do show that the proof-of-principle quasi-resonant sensor can capture wavefront aberrations without a spatial limit set by lenses. Instead, the spatial limitation is set by the 4.65 μm pixel pitch of the camera used. The wavefront was reconstructed by the use of the least-square estimate of the Zernike coefficients which is the preferred reconstruction method that reduces the level of noise.

The sensor has been speculated to have potential for challenging wavefront sensing including potential detection of exo-planets although this would still be very speculative until the concept is developed further. It has also led us to start work on metasurfaces for wavefront sensing [17] and it seems likely that with further advancement of nanostructuring of surfaces for sensing and for imaging [21] better structures for wavefront sensing can be developed.

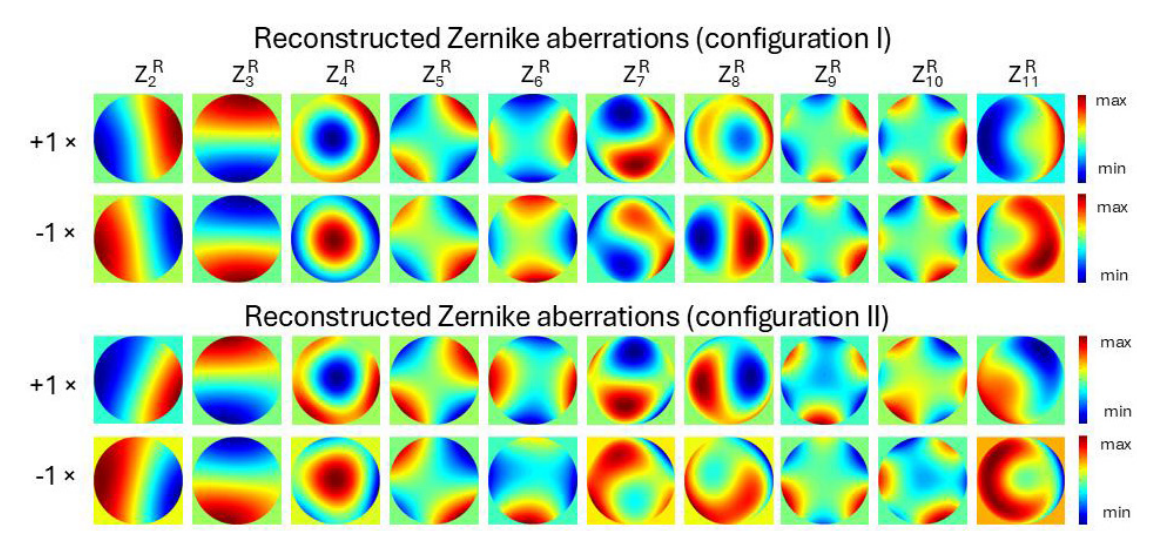


Fig 6. Reconstructed Zernike wavefronts of magnitude  $\pm 1~\mu m$  using configuration I and II, respectively, below and above the surface plasmon resonance angle. The figure has been adapted with permission from [16] © Optical Society of America.

### 5 Conclusions

Here, we have reviewed our search for intensity-based wavefront sensors using the gradients of intensity images. This approach is appealing as most often the spatial phase varies significantly whereas amplitude variations across the pupil are typically small. The waveguide-based sensor has shown potential as a flexible sensor, and the DMD-based sensor has shown potential as being easy to reconfigure in real time. However, the sensor that is likely of most relevance is the one using a quasi-resonant reflection as this opens a new pathway for phase imaging at the nanoscale with nanostructured surfaces. This could potentially replace the Hartmann-Shack wavefront sensor in many applications due to its high spatial sampling density and its adjustable dynamic range with carefully engineering of the reflectance characteristics. Further development with nanostructures could make the sensor work in transmission and with simultaneous detection of both cartesian derivatives of the wavefront.

## Acknowledgements

We wish to acknowledge the help and insight provided by Dr Alessandra Carmichael Martins in the development of the sequential scanning DMD-based HS-WFS and on its use for ophthalmic applications.

### References

- 1. Malacara D, "Optical Shop Testing", 3rd Edn, (Wiley), 2007.
- 2. Fried D L, Statistics of a geometric representation of wavefront distortion, J Opt Soc Am, 55(1965)1427–1435.
- 3. Booth M J, Neil M A A, Juškaitis R, Wilson T, Adaptive aberration correction in a confocal microscope, *PNAS* 99(2002)5788–5792.
- 4. Maeda K N, Kuroda T, Hori Y, Watanabe H, Fujikado T, Tano Y, Hirohara Y, Mihashi T, Effect of tear film break-up on higher-order aberrations measured with wavefront sensor, *Am J Ophthalmol*, 133(2002)115–117.
- 5. Ryle J P, Vohnsen B, Sheridan, J T, Simultaneous drift, microsaccades, and ocular microtremor measurement from a single noncontact far-field optical sensor, *J Biomed Opt*, 20(2015)027004; 10.1117/1.JBO.20.2.027004.
- Trujillo-Sevilla J M, González O C, Bonaque-González S, Gaudestad J, Rodríguez Ramon J M, High-resolution wavefront phase sensor for silicon wafer metrology, Proc SPIE 10925, 2019; doi.org/10.1117/12.2505764.

- Campbell H I, Zhang S, Greenaway A H, Restaino S, Generalized phase diversity for wave-front sensing, Opt Lett, 29(2004)2707–2709.
- 8. Ragazzoni R, Pupil plane wavefront sensing with an oscillating prism, J Mod Opt, 43(1996)289–293.
- 9. Akondi V, Castillo S, Vohnsen B, Digital pyramid wavefront sensor with tunable modulation, *Opt Express*, 21(2013)18261–18272.
- 10. Vohnsen B, Castillo S, Rativa D, Wavefront sensing with an axicon, Opt Lett, 36(2011)846-848.
- 11. Linnik W P, A simple interferometer for the investigation of optical systems, Proc Acad Sci USSR, 1(1933)208-210.
- 12. Akondi V, Jewel A R, Vohnsen B, Digital phase-shifting point diffraction interferometer, *Opt Lett*, 39(2015)1641–1644.
- 13. Valente D, Rativa D, Vohnsen B, Wavefront sensing using a liquid-filled photonic crystal fiber, *Opt Express*, 23 (2015)3005–13014.
- 14. Vohnsen B, Martins A C, Qaysi S, Sharmin N, Hartmann–Shack wavefront sensing without a lenslet array using a digital micromirror device, *Appl Opt*, 22(2018)E199–E204.
- 15. Martins A C, Vohnsen B, Measuring ocular aberrations sequentially using a digital micromirror device, *Micromachines*, 10(2019)117; doi.org/10.3390/mi10020117.
- 16. Vohnsen D, Valente D, Surface-plasmon-based wavefront sensing, Optica, 2(2015)1024-1027.
- 17. Vohnsen B, Valente D, Deshpande R A, Pors A, Bozhevolnyi S, Towards wavefront sensing with metamaterials, Frontiers in Optics abstract FF1G.5 (2016); doi.org/10.1364/FIO.2016.FF1G.5.
- 18. Stiles W S, Crawford B H, The luminous efficiency of rays entering the eye pupil at different points, *Proc R Soc London*, 112(1933)428–450.
- 19. Vohnsen B, Iglesias I, Artal P, Guided light and diffraction model of human-eye photoreceptors, *J Opt Soc Am A*, 22(2005)2318–2328.
- 20. Valente D, Vohnsen B, Retina-simulating phantom produced by photolithography, Opt Lett, 42(2017)4623-4626.
- 21. Priscilla N, Sulejman S B, Roberts A, Wesemann L, New avenues for phase imaging: optical metasurfaces, *ACS Photonics* 11(2024)2843–2859.

[Received: 15.06.2024; revised recd: 28.06.2024; accepted: 30.06.2024]